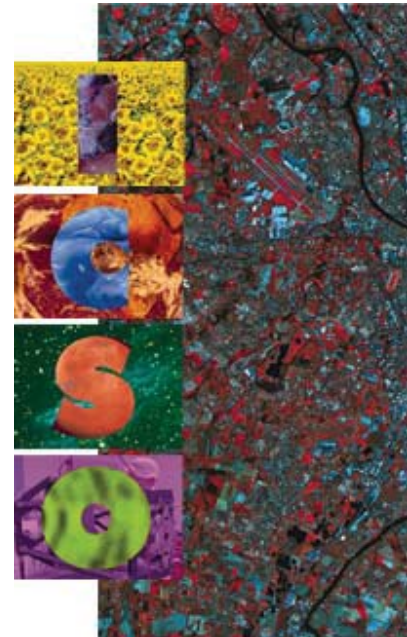


# International Conference on Space Optics—ICSO 2000

Toulouse Labège, France

5–7 December 2000

*Edited by George Otrio*



## *Aspherisation of the GALEX beam-splitter*

*Raymond Mercier, Michel Mullet, Michel Lamare*



ics0 proceedings



## ASPHERISATION OF THE GALEX BEAM-SPLITTER

Raymond MERCIER, Michel MULLOT, Michel LAMARE

*Laboratoire Charles Fabry (CNRS UMR 8501), SupOptique,  
Institut d'Optique Théorique et Appliquée,  
Centre Scientifique d'Orsay, B.P. 147, 91403 ORSAY Cedex (France)*

**RÉSUMÉ** - *Le projet GALEX vise à obtenir à la fois une imagerie directe et une spectroscopie de type prisme-objectif dans le domaine UV. Une séparatrice dichroïque assure la sélection spectrale dans deux voies: 135-180 et 180-300 nm. La conception optique de l'instrument a conduit à partager la correction des aberrations entre le télescope lui-même, la séparatrice et les fenêtres des détecteurs. Les asphérisations prévues pour les deux faces de la séparatrice étaient respectivement de 4,72 et 11,4  $\mu\text{m}$ , celle-ci a un diamètre de 110 mm (100 mm utiles) pour une épaisseur de 4mm, ce qui posait déjà un problème pour le surfacage plan. Les asphérisations ont été réalisées par érosion ionique à faisceau large, technique qui allie une bonne précision de forme à une conservation de la faible rugosité initiale obtenue lors du polissage plan des faces. Deux exemplaires ont été asphérisés et contrôlés. Les résultats des tests de ces modèles de vol permettent de penser que les défauts résiduels auront une influence faible sur la qualité de l'imagerie.*

## 1 - INTRODUCTION

The GALEX project (GALaxy evolution EXplorer) is a NASA Space Ultraviolet Small Explorer mission. It combines direct imagery along with prism-objective style spectroscopy using an original Grism specially developed by the LAM (Laboratoire d'Astronomie de Marseille, France) and Jobin-Yvon [Gran 2000]. As shown in figure 1, the GALEX telescope illuminates two detectors through a dichroic beam-splitter, giving access to two ultraviolet channels: 135-180 nm (FUV, far ultraviolet) in reflection and 180-300 nm (NUV, near ultraviolet) in transmission. The optical design of the system by the LAM had led to sharing the aberration compensation between the fairly high aperture (F/6) telescope itself, the beam-splitter (mainly correcting astigmatism) and the detector windows (correcting field curvature). The aspherisations calculated for the beam-splitter were of 4.72 $\mu\text{m}$  for the first side (named hereafter FUV side, for it reflects the light towards the FUV detector) and 11.4 $\mu\text{m}$  for the second (named hereafter NUV side, for it transmits the light towards the NUV detector). If the FUV side *only* corrects (by reflection) the incoming beam aberrations, the NUV side must *also* compensate for the aberrations introduced on the transmission by the aspherisation of the FUV side.

The 110 mm diameter beam-splitter (100 mm useful) was only 4 mm thick, that already posed a problem to the manufacturer for polishing it flat. The two aspherisations were achieved by broad beam ion milling, technique that combines a good shape precision while preserving the original smoothness allowed by the classical polishing. We shall describe the technique used for the aspherisation and the control of the process. We shall also present the results that were achieved on the two flight-model beam-splitters that were produced, and their interpretation taking into account the location of the component in the optical system.

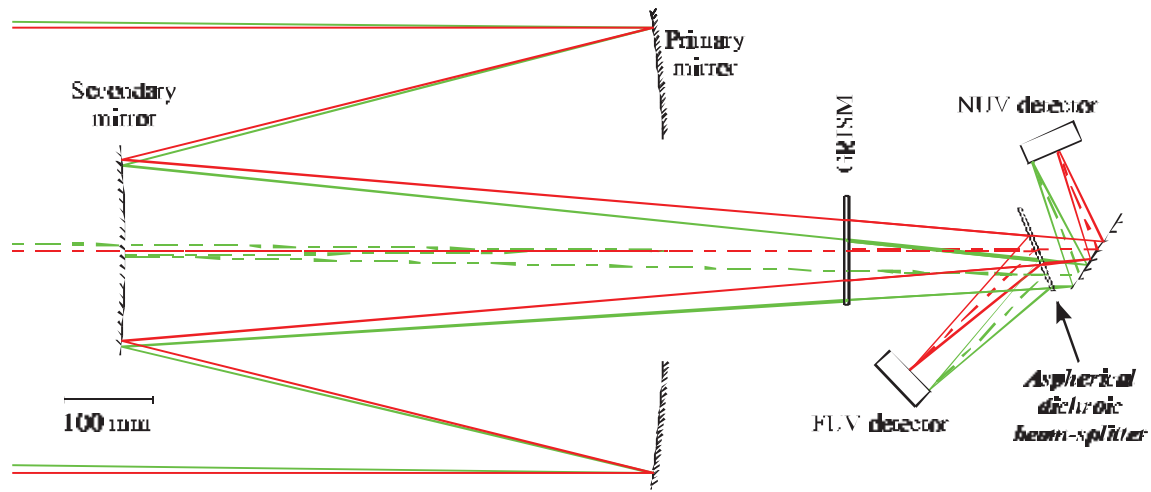


**Figure 1:** schematic diagram of the GALEX optical configuration: a high aperture (F/6) telescope, the dispersive GRISM and the aspherical dichroic beam-splitter dividing the light into two channels, reflecting the FUV (135-180 nm) and transmitting the NUV (180-300 nm)

## 2 - PRINCIPLES OF BROAD BEAM ION ASPHERISATION

This technique was developed in our laboratory instead of the more widely used small beam technique for its possibility to achieve strong amplitude aspherisations. The experimental chamber is shown in figure 2: a Kaufmann ion source generates a fairly collimated beam of argon ions. The beam has a density of  $0.5 \text{ mA/cm}^2$  of  $1 \text{ keV}$  ions. This beam is modulated radially by a mask, the aperture of which is calculated in order to give the proper erosion profile. As a first order approximation, the angular aperture at a given distance from the axis should be proportional to the required erosion. The substrate to be eroded is rotated with a constant speed to insure axisymmetric erosion. The sample holder is cooled by water circulation in order to limit temperature rising of the substrate ( $\sim 20^\circ\text{C}$  above room temperature, instead of several hundred degrees without cooling).

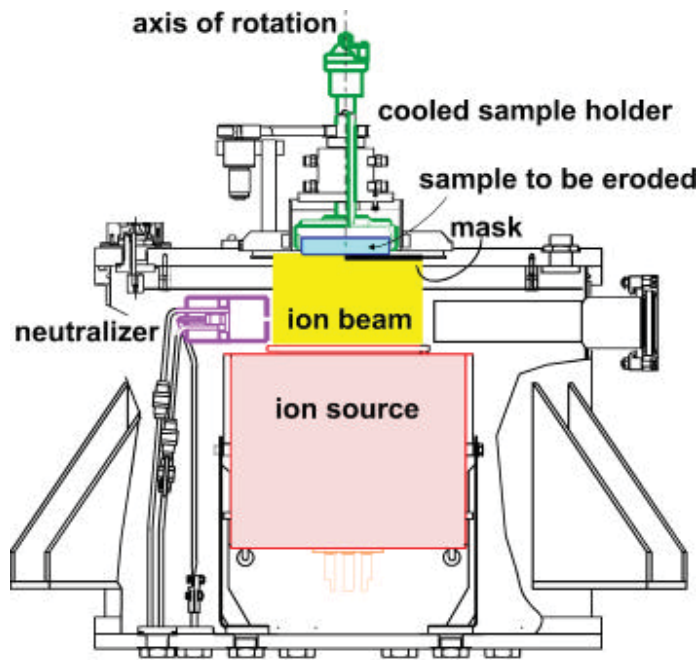


**Figure 2:** schematic diagram of the erosion set-up. The argon ion gun produces a fairly collimated beam that is modulated by the mask. The sample to be eroded is held by a rotating cooled sample holder.

### 3 - EXPERIMENTAL PROCEDURE

#### 3.1 - Mask calculation and fabrication

The masks that were used are represented in figure 3a and b, along with the aspherical erosion profiles that were required. The fine calculation of the mask is done taking into account the beam intensity profile and also the divergence of the beam and the interval between the mask and the substrate (1 mm for this project). The masks are cut out of a pyrocarbon sheet 0.5 mm thick by wire-electrical discharge machining. The precision achieved is better than  $5\mu\text{m}$ . Pyrocarbon combines the advantages of a reduced effect of mask pulverisation and a good rigidity.

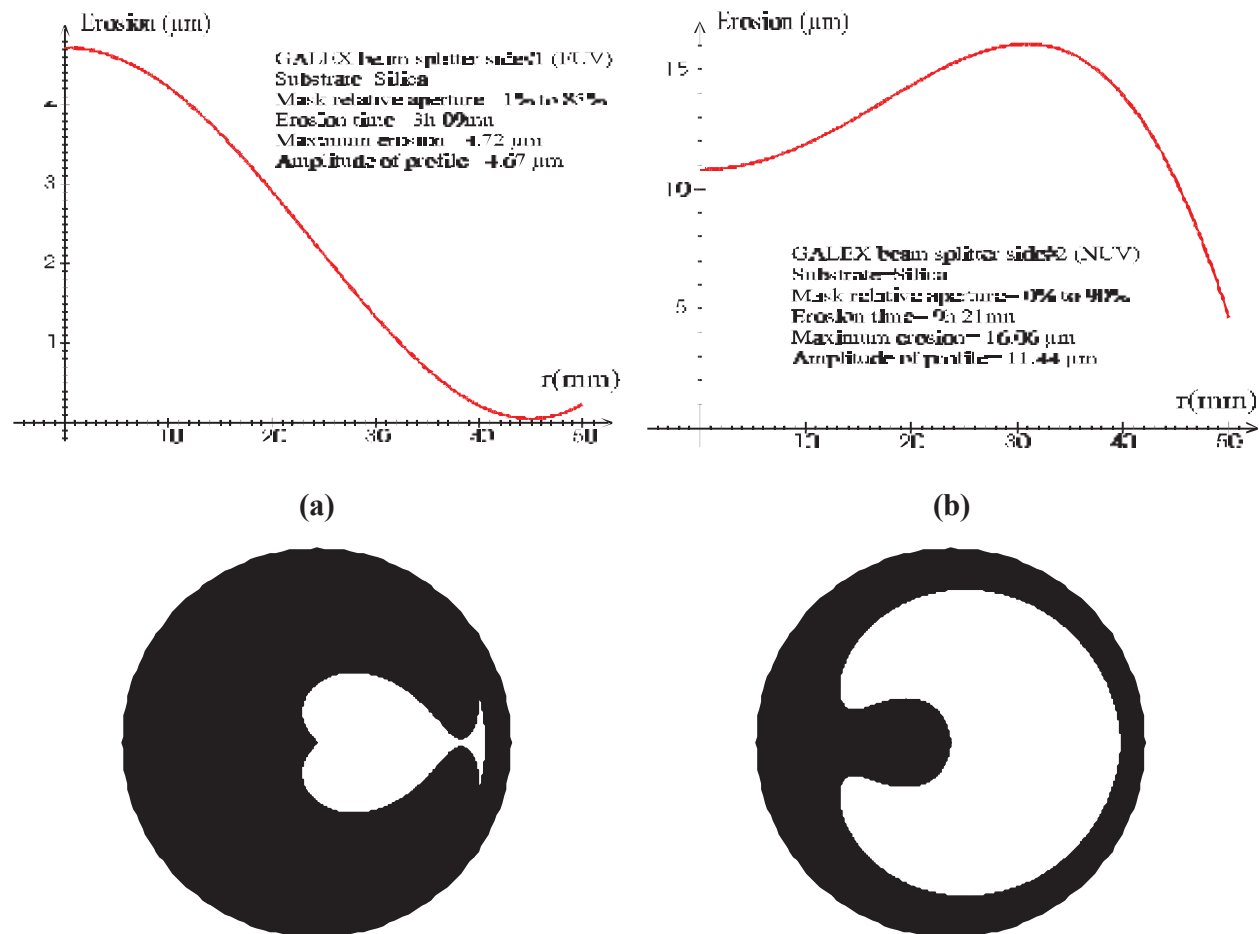


**Figure 2:** Erosion profiles and corresponding masks used to aspherise the two faces of the GALEX beam-splitter. Masks have a 120 mm outer diameter and are cut out of 0.5 mm thick pyrocarbon.

#### 3.2 - Testing the masks

Considering the difficulty of polishing the beam-splitter flat, the erosion had obviously to be thoroughly tested first. Thick silica flats were therefore polished and tested before and after erosion. Subtracting the shape before erosion from the measurement after erosion allowed determining precisely the erosion profile generated by the mask. As most axisymmetric processes, there is a severe problem in the vicinity of the axis of symmetry: this is a singular point for the process and the slightest decentering of the mask leads to very strong under- or over-erosion. Owing to the central obscuration of the telescope, this point was overlooked in the first discussions. Unfortunately, the position of the beam-splitter near to the focal plane means that the beam-splitter is used all the way to the centre, as may be seen on figure 1. So we could only do our best to reduce the defect as much as possible, both during mask calculation and positioning of the mask in the set-

up. Fortunately, this proximity to the focal plane also reduces the effect of slope errors and the final results remain quite satisfactory as will be seen below.

Figure 3 shows the result of the testing of the FUV mask:

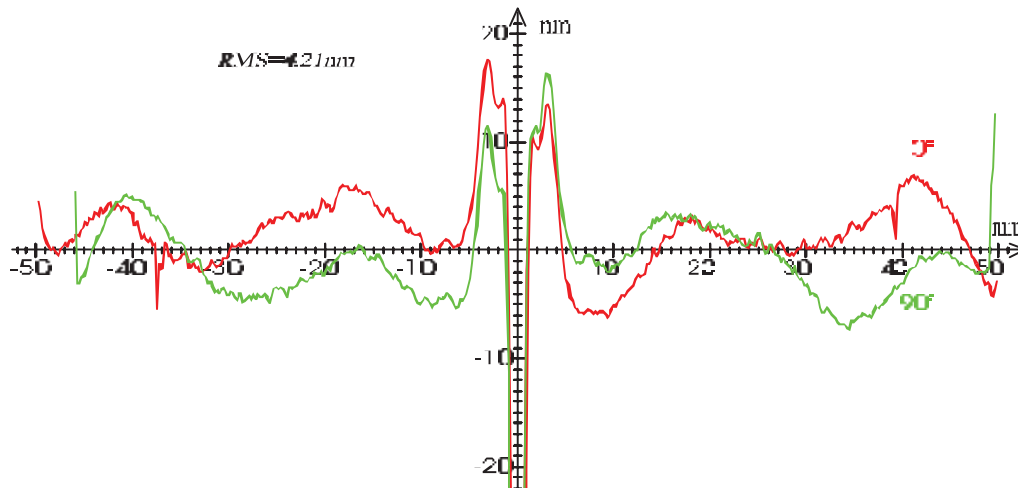


**Figure 3:** result of a 3h09mn test erosion of the FUV mask, two perpendicular profiles of erosion (corrected for the initial surface profile, 99.43% of the theoretical profile and a supplementary curvature  $R=14$  km). The main defects in amplitude are located near the centre, 99% of the surface is within 25 nm P-V.

### 3.3 - Erosion procedure

The previous tests gave the profile of the erosion effectively achieved with the masks. This was of course not exactly the required profile. Furthermore, the substrates to be eroded were not perfectly flat prior to erosion. We therefore optimised the erosion time so that adding the estimated erosion (based on the experimentally measured erosion profile) to the start-off shape of the surface would give the best possible result. This allowed to a certain extent to correct a part of the defects of the original surface, as will be confirmed by the results. This procedure was optimal for the FUV side. For the NUV side that works in transmission, it was logical to also take into account the defects of the FUV side, after erosion. We therefore eroded the NUV side *after* the erosion of the FUV: the beam splitter was tested interferometrically in transmission and, again based on the experimentally measured erosion profile, we estimated the erosion required in order to get the transmission the nearest possible to the theory. Furthermore, the amplitude of the erosion was too important to be able to achieve a sufficient precision in a single step. We therefore did the NUV erosion in two steps:  $\sim 90\%$  in a first step, then the remaining erosion could be more precisely estimated after control of the result of the first erosion. Finally, each surface was uniformly eroded (without a mask) for ten minutes, in order to remove the subsurface that may have been polluted by the deposition of matter sputtered from the carbon mask and the vacuum chamber, and thus leave an as clean as possible surface for the coating.

## 4 - TESTING THE EROSIONS AND THE FINAL COMPONENTS

### 4.1 - Surface roughness

Roughness was not systematically measured before and after erosion, for lack of time and not to multiply the risks of damaging the surface. It was only done on the test erosion of the FUV mask. Roughness measurements were performed on a Zygo 5500, giving access to the frequency domain  $\approx [2 \text{ mm}^{-1}, 500 \text{ mm}^{-1}]$ . Before erosion, the roughness varied from 1.5 to 2.5 Å RMS over the whole surface. Measured after the 3h09mn erosion, the roughness ranged from 1.5 to 2.6 Å. This

confirmed our previous experience. It is relatively important to be able to maintain these low roughness figures for the FUV side that works in reflection down to a fairly short wavelength (135 nm).

## 4.2 - Interferometric testing procedures and problems

Testing was done interferometrically, in reflection and in transmission. These tests were done using a phase-shift interferometer, basically giving a nanometre precision [Merc 97] over a 96 mm diameter pupil, working in visible He-Ne light (633 nm). Some surfaces were also tested mechanically in order to confirm the results.

Testing the beam-splitter cumulated most of the problems one may encounter, including:

- i) diameter of the sample greater than that of the interferometer
- ii) strongly deformed aspherical profiles
- iii) thickness well below the traditional requirements.

### 4.2.1 - Diameter problem

Our interferometer has a pupil of 96 mm in diameter, so the sample had to be translated to register the whole surface in several acquisitions. These individual registrations had then to be stitched-up together to obtain the whole profile.

### 4.2.2 - Strong aspheres

The FUV surface has a maximum slope of 161  $\mu\text{rd}$ ; the NUV surface has a maximum slope of 1.39 mrd. In reflection at the control wavelength of 633 nm, these slopes correspond respectively to 2 mm/fringe and 0.23 mm/fringe. Interferometer magnification being 218  $\mu\text{m}/\text{pixel}$  in order to cover the pupil with the 512x512 pixels of the CCD camera, this leads to 9 pixels/fringe and 1 pixel/fringe. Obviously, in the latter case, we could not even cover the whole surface of the interferometer pupil. So for the NUV side, it was also necessary to tilt the surface in order to register it zone by zone. This led us to stitch together nine different registrations of the NUV surface corresponding to various translations and tilts.

Another problem posed by the slopes of the NUV surface is magnification/distortion: 1.39 mrd represents a height variation of 303 nm over the width of a pixel. This required precise measurement of magnification and distortion, well below pixel size.

### 4.2.3 - Thickness of the sample

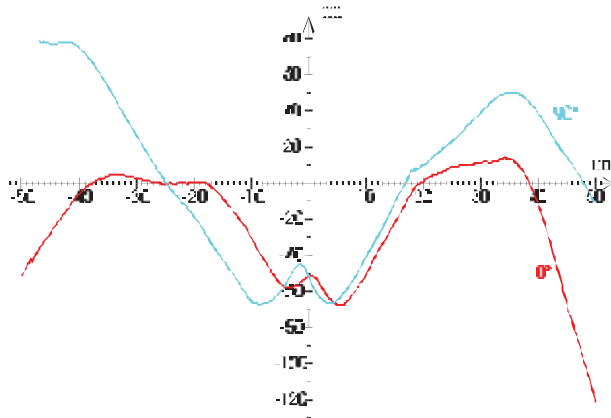
A general problem of testing such a flimsy component is holding it. As an example, uniformly resting on its periphery in a horizontal position, the natural deformation due to gravity is 60 nm. Resting horizontally on three points, the deformation rises to 210 nm. This is of course a challenge for mounting the beam-splitter in the instrument without strain (this is dealt with in another paper of this conference [Mill 2000]), but also for testing it.

The interferometer having a horizontal axis, the beam-splitter was tested in a vertical position. This avoids the important sag that appears when it is horizontal, as long as it is held perfectly symmetrically with respect to its centre of gravity. This is obviously impossible to master perfectly and we did not have the time to study and experiment a well-adapted mounting, so there remains an uncertainty on the exact shape of the beam-splitter. This uncertainty is probably rather small, as may be deduced from the comparison between reflection and transmission measurements done in section 4.3.

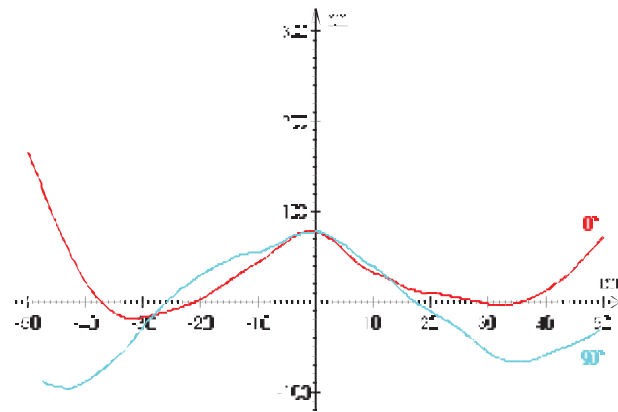
Another concern we had during this project was the risk that the beam-splitter may deform in the erosion process. The procedure define in 3.3 was based on the assumption that the erosion of the NUV side would not deform the previously eroded FUV side. This was new for us, as it was the first time we eroded *both sides* of such a *thin* component. The test was done on the "Coating path finder", aspherised on one side to do a full-scale test of the compatibility of our ion milling with the coating process. We measured the non-eroded side before and after a FUV erosion on the other side. The difference was 30 nm P-V, 5.5 nm RMS. These figures include the hypothetical effect of the erosion of the opposite side *and* the strain induced by the mechanical mount.

### 4.3 - Results of interferometric testing

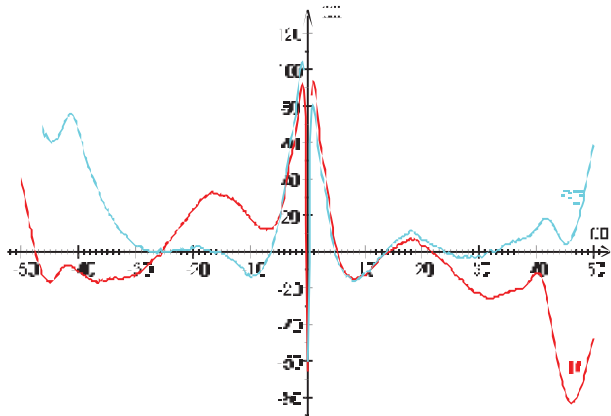
The results given here concern the second flight model to be aspherised. The results are systematically given with respect to the best sphere, the curvature of which remains well in the tolerances that were specified. Figure 4 shows two perpendicular profiles of the surfaces before and after erosion. One may notice that the "quality" of the surface has effectively improved, the erosion time taking into account the original defects of the substrate. After erosion, the departure from the theoretical profile is 27 nm RMS for the FUV side and 31 nm RMS for the NUV side. As explained above, the essential of the defects is in the central zone.



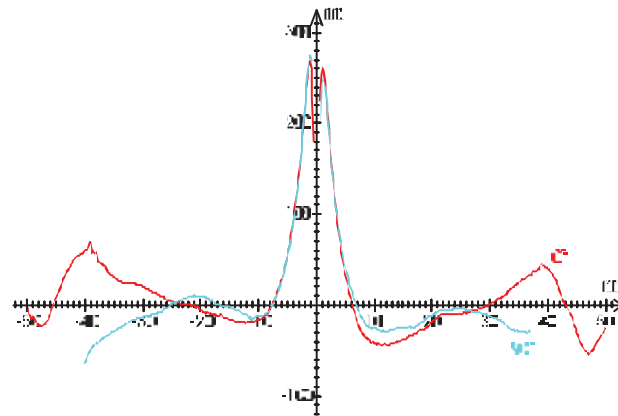
FUV side before aspherisation:  
36 nm RMS to the best sphere



NUV side before aspherisation:  
43 nm RMS to the best sphere



FUV side after 4.7 μm aspherisation:  
27 nm RMS, after correction for the theoretical profile and a 8.3 km radius of curvature



NUV side after 16 μm aspherisation:  
31 nm RMS, after correction for the theoretical profile and a 14 km radius of curvature

**Figure 4:** two perpendicular profiles of the interferometric control of the two sides of the second flight model, before and after aspherisation. Departure from the theoretical profile after aspherisation is improved with respect to the initial departure of the surface from the best sphere.

If the control in reflection of the FUV side is significant of its influence on the final instrument quality, the NUV control must take into account the transmission of the beam-splitter. This control was done by inserting the beam-splitter in a cavity in the interferometer and subtracting the profile obtained without the beam-splitter in the cavity.

The results (figure 5a) correspond to the theoretical transmission within 17 nm RMS, the essential of the defects being again localised in the central zone.

Knowing the refractive index, it is easy to deduce the transmission of the beam-splitter from the result of the tests in reflection of the two sides of the beam-splitter. As a first verification of the validity of the test process, the result may be compared with the measured transmission, as represented in figure 5b. The difference is below 4 nm RMS and is mainly due to the edge where the NUV side has very strong slopes and is therefore very sensitive to slight misalignments. However satisfactory this may be, it does not totally prove the validity of the test: in particular, this result would be unaffected by a error in the magnification. This is why we wanted to test the surfaces using an totally independent method.

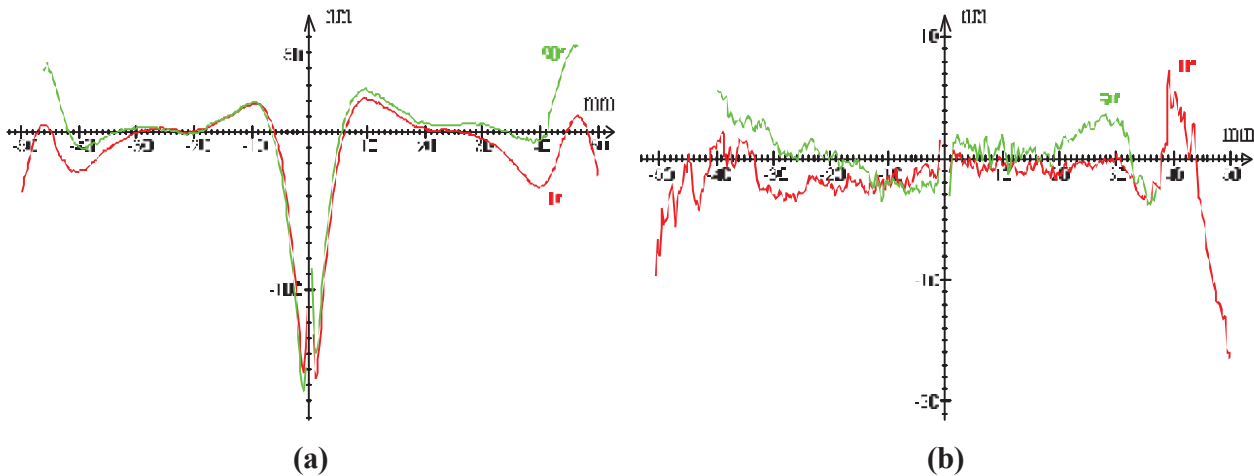


**Figure 5:** (a) difference between the measured transmission and the theoretical transmission (corrected for a 8.5 km radius of curvature) represented by two perpendicular profiles; (b) difference between the transmission deduced from the shape measurements of the two sides and the direct measurement of transmission (no curvature correction).

#### 4.4 - Comparison of interferometric and mechanical testing

As previously mentioned, interferometric measurements were partially cross-checked by mechanical measurements. This was done using a FormTalysurf mechanical profilometer. The beam-splitter then lies horizontal, resting on three steel balls at 120° in order to be able to model the sagging under the effect of gravity. The result of this comparison is given in figure 6. If the two measurement techniques were to give identical results, these differences would coincide exactly with the theoretical sag of the beam-splitter in the horizontal position, neglecting the effect of gravity on the upright position used in the interferometer. Numerically, the differences between the measurements and the theoretical profiles represent 46 nm RMS. A good deal of the difference is curvature and after correction of curvature, this value goes down to 30 nm RMS in the X-direction and 20 nm RMS in the Y-direction. Taking into account all the uncertainties (the exact location on the surface, the spurious sag in the vertical position, the modeling of the theoretical flexion in the horizontal position...) and the estimated exactitude of FormTalysurf measurements ( 100 nm P-V), the agreement seems very reasonable and tends to confirm the exactitude of the interferometric measurements, at least as to magnification.

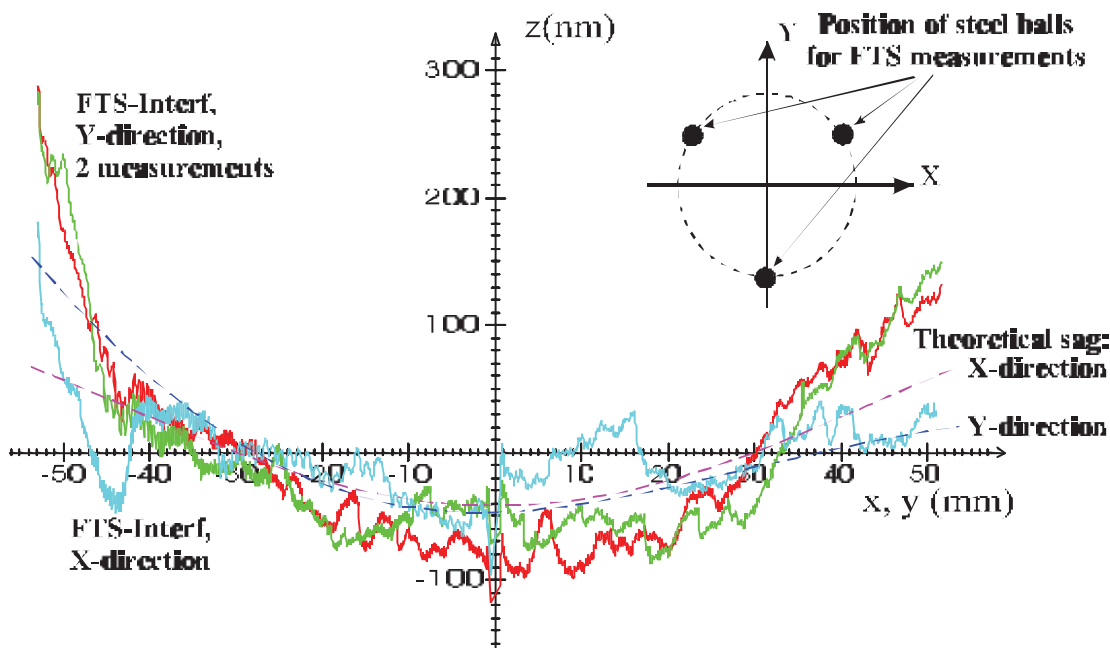


**Figure 6:** Comparison between interferometric and mechanical measurements of the NUV side of the Flight Model 2 of the GALEX beam splitter. The continuous curves represent the difference between the FormTalysurf (FTS) and the interferometric measurements, in two perpendicular directions (Y is symmetrical with respect to the three steel balls, as indicated in the insert). Dashed lines show the theoretical sag of the beam-splitter through gravity.

## 5 - INTERPRETATION OF THE TESTING: INFLUENCE ON THE INSTRUMENT

The position of the beam-splitter near to the focal plane of the instrument makes the interpretation of the defects in terms of image degradation somewhat different from the more common situation, when the surface is near the pupil. In the case of GALEX, the intersection of the image aperture cone by the beam-splitter is 35 mm in diameter, with an 18 mm diameter unused central zone. For the beam-splitter, this is an annular sub-pupil, the position of which varies with the position of the object in the field. Analysing the results of the testing of the beam-splitter must therefore be done in two steps. For a varying position of the annular sub-pupil on the beam-splitter, we must determine:

- i) the average slope of the wavefront in the sub-pupil: multiplied by the distance to the focal plane, this slope will define the local displacement of the image (corresponding to a local distortion)
- ii) the departure of the wavefront from the mean plane; this term is a bit more delicate to interpret. As will be seen, the maximum influence on the FUV reflected wavefront is 40 nm RMS. If it was the only source of defects, and although it would not be possible to consider the optics as diffraction limited (Maréchal's criterion gives  $\lambda_{\text{working}}/14 \sim 10$  nm RMS), it would be nearer to the diffraction regime than the geometric regime. We would then only consider the RMS influence of the defects on the wavefront. But, as the aberrations of the telescope represent several wavelengths, the whole instrument will probably be working more in the geometrical regime and it is the influence of the beam-splitter on the slope of individual rays that would be more significant. In a first step, we shall consider departures from the best plane.

The analysis was carried out on the two beam-splitters. Numerical values are given in the table I, local distortion is expressed both in angular and linear terms, the latter taking into account the 200 mm distance between the beam-splitter and the focal plane. It also gives the worst value of the departure of the reflected (FUV) and transmitted (NUV) wavefront from the best plane. Figures 7 and 8 show the spatial variation of these parameters in the field of the telescope, i.e. when the annular sub-pupil explores the whole useful surface of the beam-splitter.

Beam-splitter sample n°	FUV channel			NUV channel		
	Local distortion		Worst wavefront departure	Local distortion		Worst wavefront departure
	Angular	Linear in focal plane		Angular	Linear in focal plane	
#1	1.9 $\mu$ rd RMS, 3.6 $\mu$ rd max.	0.4 $\mu$ m RMS, 0.7 $\mu$ m max.	32 nm RMS	2.1 $\mu$ rd RMS, 3.9 $\mu$ rd max.	0.4 $\mu$ m RMS, 0.8 $\mu$ m max.	49 nm RMS
#2	2.5 $\mu$ rd RMS, 6.4 $\mu$ rd max.	0.5 $\mu$ m RMS, 1.3 $\mu$ m max.	40 nm RMS	0.76 $\mu$ rd RMS, 1.6 $\mu$ rd max.	0.15 $\mu$ m RMS, 0.3 $\mu$ m max.	27 nm RMS

**Table I:** measured values of RMS and maximum local distortion of the image and worst wavefront for the two channels (FUV in reflection and NUV in transmission) for the two samples of the beam-splitter to be eroded.

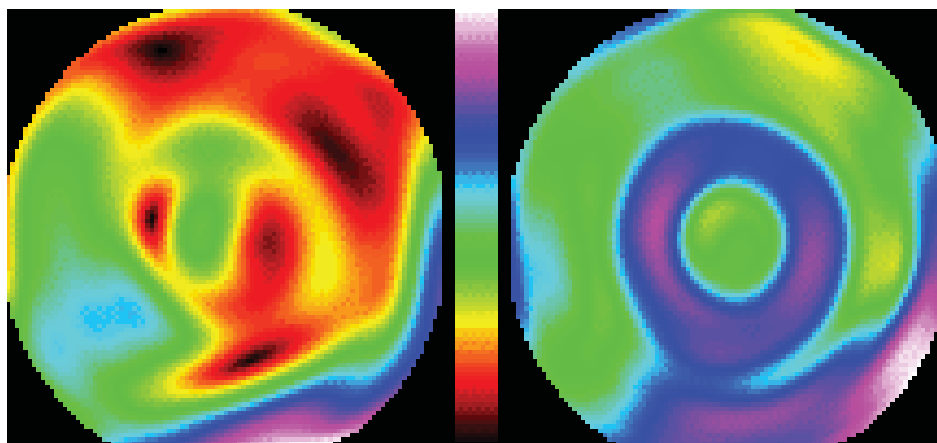


**Figure 7:** Imagery in the FUV channel (light reflected by the FUV side): map of the local slopes of the best plane (left, full-scale=6.4  $\mu$ rd, gives the local distortion if multiplied by the distance to the image plane) and map of the departures RMS from this best plane (right, full-scale=40 nm RMS) of the sub-aperture wavefront over the field of the instrument.

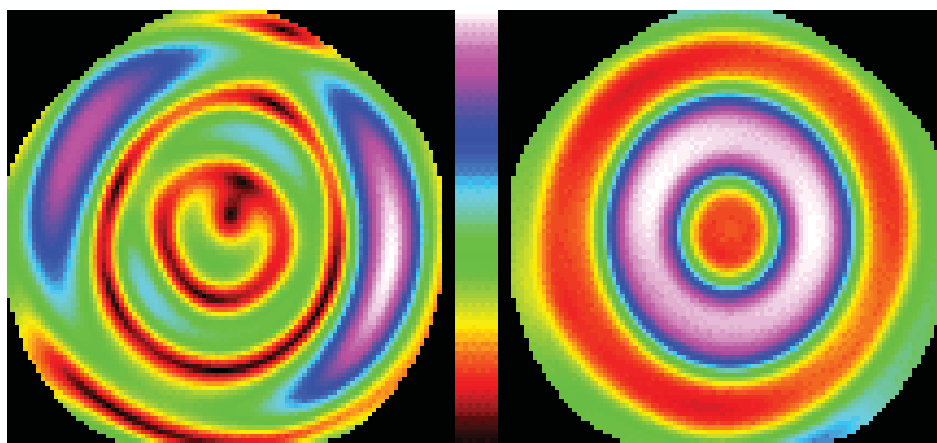


**Figure 8:** Imagery in the NUV channel (light transmitted by the beam-splitter): map of the local slopes of the best plane (left, full-scale=1.6  $\mu$ rd) and map of the departures RMS from this best plane (right, full-scale=27 nm RMS) of the sub-aperture wavefront over the field of the instrument.

The first conclusion is that the local distortion is in the micron range, so it is well below pixel size and may be considered as negligible. Departure of the wavefront would have to be compared to the true aberrations of the rest of the instrument, but we do not have access to this data. The only figure we have is the global goal: 80% of the energy in 2.3 arc-seconds diameter. Converted to the plane of the beam-splitter, this angle corresponds to a radius of 84  $\mu\text{rd}$ . We may compare this to the measurements we did on the two samples, using both the diffraction and the geometrical approach:

i) diffraction approach: assuming all the rest of the instrument to be perfect, we calculated by Fourier transform the angular radius corresponding to 80% of encircled energy. We obtained values ranging from 20 to 27  $\mu\text{rd}$  for the FUV channel and from 19 to 31  $\mu\text{rd}$  in the NUV channel. These values (calculated for the worst sub-pupil) must be compared the overall tolerance for the instrument (84  $\mu\text{rd}$  seen from the beam-splitter) and also to what one would obtain with pure diffraction (no aberrations): 8 to 10.5  $\mu\text{rd}$  in the FUV channel and 10.5 to 17.5  $\mu\text{rd}$  in the NUV.

ii) geometrical approach: we now consider the influence of the defects on the slope of the geometrical rays. We have calculated the RMS slope errors introduced by the defects and the percentage of the rays corresponding to a slope less than this value. We obtained 12 to 17  $\mu\text{rd}$  RMS, corresponding to 71 to 86 % of the energy. The geometrical influence of the beam-splitter therefore represents 14 to 20% of the overall error budget, and this is for the worst sub-pupil.

Whatever the approach, our conclusion is that the beam-splitter should only have a small impact on the final quality of the telescope. This result was allowed by broad beam ion milling (low roughness, good shape precision even for such a thin component) and would have probably been unattainable with any other method.

## ACKNOWLEDGEMENTS

We wish to thank warmly J. Flamand, R. Grange and B. Millard for having drawn us into this adventure. The results would not have been the same without the care with which Mr Boyadjian of the Shahum Company did the cutting-out of the masks.

## BIBLIOGRAPHY

[Gran 2000] R. Grange, B. Milliard, J. Flamand, "GALEX UV Grism for slitless spectroscopy survey", ICSO 2000

[Merc 97] R. MERCIER, M. LAMARE, P. PICART, J.-P. MARIOGE, "Two-flat method for bi-dimensional measurement of absolute departure from the best sphere", Pure Appl. Opt., 1997, **6**, pp. 117-126 and R. MERCIER, M. LAMARE, "Experimental comparison of the two- and the three-flat methods for absolute optical surface testing", Pure Appl. Opt., 1997, **6**, pp. 773-777

[Mill 2000] B. Milliard, R. Grange, C. Martin, "GALEX: a UV telescope to map the star formation history of the universe", ICSO 2000